Kasetsart J. (Nat. Sci.) 40 : 795 - 808 (2006)

Numerical Study on the Strongly Swirling Aerodynamic Field in an Isothermal Vortex Combustor

Smith Eiamsa-ard[1]* and Pongjet Promvonge[2]

ABSTRACT

This research presented the application of a mathematical model for simulation of turbulent strongly swirling confined flow in an isothermal vortex combustor. Computations, based on a finite volume method, were carried out by utilizing the standard *k-ε* model and a simplified Algebraic Reynolds Stress Model (ASM) together with three discretization schemes, namely upwind, hybrid and QUICK. The work was performed in order to provide an understanding of physical behaviour of the swirling flow in a cold model vortex combustor. The ASM for steady compressible flows was used to predict the flow and was compared with the *k-ε* turbulence model. The calculated axial and tangential velocity profiles were compared with available measurement data. The mean flow patterns were shown in terms of contour plots. The prediction result showed that the ASM was better than standard *k-ε* model and the ASM together with QUICK results gave good agreement with the measurement data. Moreover, influences of the grid mesh distribution and the value of β were also studied.

Key words: strongly swirling confined flow, vortex combustor, ASM, k-ε turbulence model, upwind, hybrid, QUICK

INTRODUCTION

The vortex combustor (VC) concept was germinated from the basic understanding of the strongly swirling gas-solid flows and combustion in vortex chambers. It integrates many advantages of cyclone combustor, multistage combustor, swirl burner, pulverized coal fired combustor, and fluidized-bed combustor while eliminates most of their inherent disadvantages. In combustion systems, the design of strong vortex-flows of air and fuel can have large-scale effects on entrainment and decay, heat and mass transfer, flame stability and pollutant abatement reactions. The vortex-generating system is developed by tangentially entering combustion air into the combustor. A series of combustion air injection nozzles are mounted vertically along the wall of combustor. In this combustor, all of the air is introduced tangentially into the combustor.

Swirl has been used in combustion systems to enhance the flame stability, the mixing and heat transfer besides prolonging the fuel residence time and abating the pollutants (Gupta, *et al*., 1984). This is because under appropriate conditions, swirl can be employed to induce a

[1] Department of Mechanical Engineering, Faculty of Engineering Mahanakorn University of Technology, Bangkok 10530, Thailand.

[2] Department of Mechanical Engineering, Faculty of Engineering King Mongkut's Institute of Technology Ladkrabang, Bangkok 10520, Thailand.

* Corresponding author, e-mail: smith@mut.ac.th

Received date : 13/12/05 Accepted date : 24/04/06

central recirculation zone. The re-circulating flow generates additional turbulence in the shear layer between the reverse flow and the surrounding forward flow and helps to stabilize the flame in combustors. Swirling turbulent flows are physically complex in nature due to the effect of a swirl-turbulence interaction. The turbulence structure in swirling turbulent flows is generally highly non-isotropic and non-homogeneous. Computation of swirling flows is a difficult and challenging task. Large velocity gradients appear in these flows, so numerical problems and turbulence modelling play a significant role in their analysis. The commonly used, the k-ε model may not be suitable for simulating swirling turbulent flows (Boysan *et al.*,1982). It is also found that the use of modified k-ε models or even the non-linear k-ε model (Nieh and Zhang, 1992) leads to no significant improvement of the predictions in swirling flows. The second-order moment closure models, i.e., the Reynolds Stress Model (RSM) and the Algebraic Reynolds Stress Model (ASM) provide better methods for the simulation of swirling turbulent flows (Chen, 1986; Hogg and Leschziner, 1989; Jones and Pascau, 1989) but sometime, the original ASM based on Rodi's approximation can not give satisfactory results for certain aspects of swirling flows (Nieh and Zhang, 1992). The RSM is regarded as the most logical approach to the turbulence closure problem, which does not need any ad hoc modification for extra strain rates. However, in the prediction of swirling flows with the RSM, it is necessary to solve a total of 11 governing differential equations of elliptic type: a continuity equation, three momentum equations, an ε-equation, and six equations for the Reynolds stresses. This leads to much extra computational effort to solve six Reynolds stress transport equations simultaneously (Chen, 1986; Hogg and Leschziner, 1989; Jones and Pascau 1989) and much attention needs to be paid to numerical stability and inlet boundary conditions. It is for this reason that a simplified algebraic Reynolds stress turbulence model in axisymmetric cylindrical co-ordinates is employed for simulating strongly swirling flows. The main goal of the present investigation was to evaluate the capability of the k-ε turbulence model and ASM to predict the swirling flow behaviours in a cold flow vortex combustor (Zhang *et al.*, 1992). Influences of the scheme, grid mesh distribution *(30x15, 40x20 and 47x25 points)*, and the value of β *(between 0.2 and 0.8)* are reported in this paper.

MATERIALS AND METHODS

1. Governing equations

The governing equations for constant density, isothermal flows consist of the conservation of mass and momentum. The time-averaged incompressible Navier-Stokes equations in the Cartesian tensor notation can be written in the following form:

$$\frac{\partial}{\partial x_i}(\rho u_i) = 0 \tag{1}$$

$$\frac{\partial(\rho u_i u_j)}{\partial x_j} = -\frac{\partial p}{\partial x_i} + \frac{\partial}{\partial x_j}(\bar{t}_{ij} + T_{ij}) \tag{2}$$

The mean viscous stress tensor is approximated as:

$$\bar{t}_{ij} = \mu\left(\frac{\partial u_i}{\partial x_j} + \frac{\partial u_j}{\partial x_i}\right) \tag{3}$$

where μ is laminar viscosity. The time-averaged Reynolds stress tensor, τ_{ij} $(= -\overline{\rho u_i' u_j'})$ in the above equation is not known and thus, models are needed to assign values to it or to express it in terms of the solution variables. In the present study, two turbulence closure models were used, namely the standard k-ε model and an algebraic stress model or an algebraic second moment closure (ASM). The k-ε model has already been reviewed in many references (Gatski, 1996) and it would be described only briefly.

In the standard k-ε model the Reynolds stress is linearly related to the mean rate of strain by a scalar eddy viscosity. The standard version relates the turbulent eddy viscosity to the turbulence kinetic energy k and the dissipation rate ε through Boussinesq's approximation as:

$$\tau_{ij} = -\frac{2}{3}\delta_{ij}(\rho k) + \mu_t\left(\frac{\partial u_i}{\partial x_j} + \frac{\partial u_j}{\partial x_i}\right) \quad (4)$$

where $\mu t = pC\mu\, k^2/\varepsilon$ is the turbulent eddy viscosity and e is the dissipation rate of Turbulence Kinetic Energy (TKE).

The modelled equation of the TKE, k is given by:

$$\frac{\partial}{\partial x_j}(\rho u_j k) = \frac{\partial}{\partial x_j}\left[\frac{\mu_e}{\sigma_k}\frac{\partial k}{\partial x_j}\right] + G - \rho\varepsilon \quad (5)$$

Similarly the dissipation rate of TKE is given by the following equation:

$$\frac{\partial}{\partial x_j}(\rho u_j \varepsilon) = \frac{\partial}{\partial x_j}\left[\frac{\mu_e}{\sigma_\varepsilon}\frac{\partial \varepsilon}{\partial x_j}\right] + \frac{\varepsilon}{k}\left(C_{\varepsilon 1}G - C_{\varepsilon 2}\rho\varepsilon\right) \quad (6)$$

in which G represents the rate of generation of TKE while $\rho\varepsilon$ is its destruction rate. G is given by:

$$G = \mu_e\left[\frac{\partial u_i}{\partial x_j} + \frac{\partial u_j}{\partial x_i}\right]\frac{\partial u_i}{\partial x_j} \quad (7)$$

The boundary values for the turbulent quantities near the wall are specified with the wall function method. C_μ, $C_{\varepsilon 1}$, $C_{\varepsilon 2}$, σ_k, and σ_e are empirical constants in the turbulent transport equations.

For an RSM, Reynolds-averaged transport equations can be solved for the Reynolds stress tensor, τ_{ij}, the modelled equations for which are:

$$\frac{\partial \tau_{ij}}{\partial t} + \frac{\partial(u_k \tau_{ij})}{\partial x_k} = -G_{ij} - \Phi_{ij} + \frac{\partial T_{ijk}}{\partial x_k} + \varepsilon_{ij} \quad (8)$$

where

$$G_{ij} = \rho P_{ij} = -\left(\rho\overline{u_i' u_k'}\frac{\partial u_j}{\partial x_k} + \rho\overline{u_j' u_k'}\frac{\partial u_i}{\partial x_k}\right)$$

$$\Phi_{ij} = -C_1\frac{\rho\varepsilon}{k}\left(\overline{u_i' u_j'} - \frac{2}{3}k\delta_{ij}\right) - C_2\left(G_{ij} - \frac{2}{3}G\delta_{ij}\right)$$

$$T_{ijk} = C_s\frac{\rho k}{\varepsilon}\overline{u_k' u_l'}\frac{\partial \overline{u_i' u_j'}}{\partial x_l}$$

$$\varepsilon_{ij} = \frac{2}{3}\rho\varepsilon\delta_{ij}$$

in which C_s, C_1, and C_2 are model constants.

In equation (8), from left to right, there are have the time rate of change of the Reynolds stress at a fixed point, the net convection of Reynolds stress by the mean flow to the fixed point, local production (G_{ij}) of Reynolds stress, local pressure strain (Φ_{ij}), net diffusive transport ($T_{ijk,k}$) of Reynolds stress to a fixed point, and local dissipation tensor.

2. Algebraic Reynolds Stress Model (ASM)

The ASM is derived from the Reynolds stress transport equations that relate the individual stresses to the mean velocity gradients, the turbulence kinetic energy, k, and its dissipation rate, ε, by way of algebraic expressions described below in some detail. The ASM was obtained by applying certain assumptions to the Reynolds-stress transport equations to allow the convection and diffusive gradient terms to be represented by non-gradient terms. For simplicity in solving the six Reynolds stresses, Rodi's approximation (Rodi, 1976) was used in this study and the Reynolds stress transport could be expressed in algebraic form as follows:

$$\frac{D\tau_{ij}}{Dt} - T_{ijk,k} = \frac{\tau_{ij}}{\rho k}\left(\frac{Dk}{Dt} - T_{kk,k}\right) \quad (9)$$

Substitution of equations (5) and (8) into equation (9) gives the desired algebraic expression for τ_{ij}: $-G_{ij} - \Phi_{ij} + \frac{2}{3}\delta_{ij}p\varepsilon = \frac{T_{ij}}{pk}(G - p\varepsilon)$ (10)

Rodi's approximation is appropriate only in the Cartesian co-ordinate system and may not be completely valid under co-ordinate

transformation. Boysan *et al*. (1983) suggested that some of the additional non-gradient convective stress terms arising from the transformation to the cylindrical co-ordinate system might be large relative to the gradient convective stress terms in swirling flow systems. They recommended that the non-gradient convection terms, which were functions of the mean tangential velocity in cylindrical co-ordinates, should be retained or added in the model as extra production terms. The ASM expressions can thus be written as:

$$\frac{\rho\overline{u_i'u_j'}}{\rho k}(G-\overline{\rho}\varepsilon)+\psi A_{ij}=G_{ij}+\Phi_{ij}-\frac{2}{3}\delta_{ij}\rho\varepsilon \qquad (11)$$

where Aij is the "added" convection quantity excluded from Rodi's approximation and its associated coefficient, ψ, is an arbitrary constant between zero and one.

$$A_{ij}=\begin{vmatrix} 0 & -\overline{\rho u'w'}\frac{w}{r} & \overline{\rho u'v'}\frac{w}{r} \\ -\overline{\rho u'w'}\frac{w}{r} & -2\overline{\rho v'w'}\frac{w}{r} & \left[\overline{\rho v'v'}-\overline{\rho w'w'}\right]\frac{w}{r} \\ \overline{\rho u'v'}\frac{w}{r} & \left[\overline{\rho v'v'}-\overline{\rho w'w'}\right]\frac{w}{r} & 2\overline{\rho v'w'}\frac{w}{r} \end{vmatrix} \qquad (12)$$

Thus,

$$\left[\frac{\rho\overline{u_i'u_j'}-(2/3)\delta_{ij}\rho k}{k}\right]=\frac{\lambda}{\varepsilon}\left(G_{ij}-(2/3)\delta_{ij}G-\beta A_{ij}\right)$$

or

$$\rho\overline{u_i'u_j'}=\frac{2}{3}\delta_{ij}\rho k+\frac{\lambda k}{\varepsilon}\left(G_{ij}-\frac{2}{3}\delta_{ij}G-\beta A_{ij}\right) \qquad (13)$$

where the empirical constants l and b are defined as:

$$\lambda=\frac{1-C_2}{C_1-1+\frac{G}{\rho\varepsilon}} \quad \text{and} \quad \beta=\frac{\psi}{1-C_2} \qquad (14)$$

Equation (13) provides an algebraic expression for each of the six Reynolds stresses. These six simultaneous stress-equations were solved along with the equations of turbulence kinetic energy and its dissipation rate. The first implementation of an implicit form of the algebraic relationships conducted by Rodi (Rodi, 1976) led to a non-constant coefficient C_μ in the eddy-viscosity definition which was a function of the turbulent production and dissipation rate. The implicit nature of the algebraic relationship requires that at each iteration step, an additional inner iteration was needed to solve for the appropriate τ_{ij} components. This iterative process could cause solution divergence, and increased numerical overhead because of the extensive matrix inversions required at different iteration levels. The above implicit ASM expressions can be simplified to obtain an explicit set that can be solved easily, as proposed by Zhang *et al*. (1992) and Zhang and Nieh (1992), for application to a strongly swirling flow, e.g. a cyclonic flow. The details of this are given in the following section.

3. Simplified ASM for 2D axisymmetric flows with high swirl

Experimental studies showed that, in an axisymmetric flow with high swirl, generally w >> v, u >> v and / r >> / x in almost the entire flow field. Hence, the terms containing u/ x, v/ x, w/ x, v/ r and v/r were negligible when compared with the terms containing u/ r , w/ r , and w/r. The original algebraic equations could therefore be simplified in an explicit form as shown in equation (15) below.

The turbulence kinetic energy and dissipation equations retained the same form as the parallel two-equation model based on Boussinesq hypothesis but different expressions were used for the generation term of the k-equation.

$$\rho\overline{u'v'} = -\mu_{t,xr}\frac{\partial u}{\partial r}$$

$$\rho\overline{v'w'} = -\mu_{t,r\theta}\, r\frac{\partial}{\partial r}\left(\frac{w}{r}\right)$$

$$\rho\overline{u'w'} = -\lambda\frac{k}{\varepsilon}\rho\overline{u'u'}\frac{\partial w}{\partial x} - \lambda\rho\frac{k}{\varepsilon}\left(\overline{v'v'}\frac{\partial w}{\partial r} + \beta\frac{w}{r}\overline{u'v'} + \frac{\partial u}{\partial r}\overline{v'w'}\right) \quad (15)$$

$$\rho\overline{u'u'} = \frac{2}{3}\rho k + \frac{2}{3}\rho\lambda\frac{k}{\varepsilon}\left(2\frac{\partial u}{\partial r}\overline{u'v'} + r\frac{\partial}{\partial r}\left(\frac{w}{r}\right)\overline{v'w'}\right)$$

$$\rho\overline{v'v'} = \frac{2}{3}\rho k + \frac{2}{3}\rho\lambda\frac{k}{\varepsilon}\left(\frac{\partial u}{\partial r}\overline{u'v'} + \frac{\partial w}{\partial r} + (2+3\beta)\frac{w}{r}\overline{v'w'}\right)$$

$$\rho\overline{w'w'} = \frac{2}{3}\rho k + \frac{2}{3}\rho\lambda\frac{k}{\varepsilon}\left(\frac{\partial u}{\partial r}\overline{u'v'} - 2\frac{\partial w}{\partial r} + (1+3\beta)\frac{w}{r}\overline{v'w'}\right)$$

in which

$$\mu_{t,xr} = \frac{b_1 - a_1 b_2\, r\frac{\partial}{\partial r}\left(\frac{w}{r}\right)}{1 - a_1 a_2\frac{\partial u}{\partial r}\, r\frac{\partial}{\partial r}\left(\frac{w}{r}\right)} \quad (16)$$

$$\mu_{t,rq} = \frac{b_2 - a_2 b_1\frac{\partial u}{\partial r}}{1 - a_1 a_2\frac{\partial u}{\partial r}\, r\frac{\partial}{\partial r}\left(\frac{w}{r}\right)} \quad (17)$$

where

$$a_1 = \frac{\lambda\left(\frac{k}{\varepsilon}\right)^2\left(\frac{7}{3} + 3\beta\right)\frac{w}{r} + \frac{2}{3}\frac{\partial w}{\partial r}}{1 + \lambda\left(\frac{k}{\varepsilon}\right)^2\left(\frac{2}{3}\frac{\partial u}{\partial r}\right)^2 + (1+\beta)\frac{w}{r}\frac{\partial w}{\partial r} + (1+\beta)\beta\left(\frac{w}{r}\right)^2}$$

$$a_2 = \frac{\frac{2}{3}\lambda\left(\frac{k}{\varepsilon}\right)^2\frac{\partial u}{\partial r}}{1 + \frac{2}{3}\lambda\left(\frac{k}{\varepsilon}\right)^2\left(\frac{\partial w}{\partial r}\right)^2 + (4+6\beta)\frac{w}{r}\frac{\partial w}{\partial r} + (1+6\beta+6\beta^2)\left(\frac{w}{r}\right)^2}$$

$$b_1 = \frac{\frac{2}{3}\lambda\rho\frac{k^2}{\varepsilon}}{1 + \lambda\left(\frac{k}{\varepsilon}\right)^2\left(\frac{2}{3}\frac{\partial u}{\partial r}\right)^2 + (1+\beta)\frac{w}{r}\frac{\partial w}{\partial r} + (1+\beta)\beta\left(\frac{w}{r}\right)^2}$$

$$b_2 = \frac{\frac{2}{3}\lambda\rho\frac{k^2}{\varepsilon}}{1 + \frac{2}{3}\lambda\left(\frac{k}{\varepsilon}\right)^2\left(\frac{\partial w}{\partial r}\right)^2 + (4+6\beta)\frac{w}{r}\frac{\partial w}{\partial r} + (1+6\beta+6\beta^2)\left(\frac{w}{r}\right)^2}$$

The model constant, λ, was found to be 0.135. If C_2 was taken as 0.55 and ψ varied between 0.0 and 1.0, equation (14) gave the value of β between 0.0 and 2.2.

4. Common form for the equations

All the governing partial differential equations could be re-organised and expressed in a standard form that included the convection, diffusion, and source terms for 2-D axisymmetric flows as follows:

$$\frac{\partial}{\partial x}\left(\overline{\rho}\tilde{u}\varphi\right) + \frac{1}{r}\frac{\partial}{\partial r}\left(r\overline{\rho}\tilde{v}\varphi\right) - \frac{\partial}{\partial x}\left(\Gamma_{\varphi x}\frac{\partial\varphi}{\partial x}\right) - \frac{1}{r}\frac{\partial}{\partial r}\left(r\Gamma_{\varphi r}\frac{\partial\varphi}{\partial r}\right) = S_\varphi \quad (18)$$

where ϕ, $\Gamma_{\phi x}$, $\Gamma_{\phi r}$ and S_ϕ represent the generalised variables, the exchange coefficients in x and r directions and the source terms, respectively.

5. Solution procedure

In the present computation, the time-averaged Navier-Stokes equations, equations (1) and (2); the TKE equation, equation (5); the TKE dissipation rate equation, equation (6) were solved numerically by a control-volume finite-difference method together with the turbulence model equations, equation (4) for the k-ε model or equation (16b) for the ASM. The SIMPLE algorithm was utilised for pressure-velocity de-coupling and iteration (Patankar, 1980). The discretization of the governing equations was accomplished by means of the Quadratic Upstream Interpolation for Convective Kinematics (QUICK) scheme and the source term linearisation on a staggered grid cell. The underrelaxation iterative TDMA line-by-line sweeping technique was used for solving the resultant finite-difference equations.

Due to the highly non-linear and coupling features of the governing equations for swirling flows, lower underrelaxation factors

ranging from 0.005 to 0.1 were chosen for the three velocity components to ensure the stability and convergence of the iterative calculation. Wall function was used for calculating wall shear stresses at the grid nodes along the walls. The exit boundary was chosen at the center tube outlet where zero gradient conditions were adopted for all variables except the axial velocity u, which was subject to continuity constraints. The computation was carried out using a PC computer. About 20,000 iterations were needed to achieve satisfactory convergence for each calculation case, which required about 3 hr of computer time.

6. Validotion of ASM

A strongly swirling flow in a vortex combustor (Zhang *et al*., 1992) was selected for the validation of the ASM. A schematic diagram of the vortex combustor is shown in Figure 1. It comprised a 0.11 m diameter central tube, concentrically placed inside a cylindrical chamber of 0.66 m height and 0.25 m diameter. The centre tube was set 0.51 m into the chamber. Air injected into the chamber tangentially through 3 sets of nozzles spirally ascended through the annular space and exhausted through the central tube. The measured swirl number (S) was 13.9. The specifications of the combustor are summarised in Table 1.

RESULTS AND DISCUSSION

Simulations of the isothermal swirling flow in a vortex combustor by (1) standard k-ε model and (2) simplified Algebraic Reynolds Stress Model (ASM) using three difference schemes: upwind, hybrid and QUICK, are presented and validated with measurement data

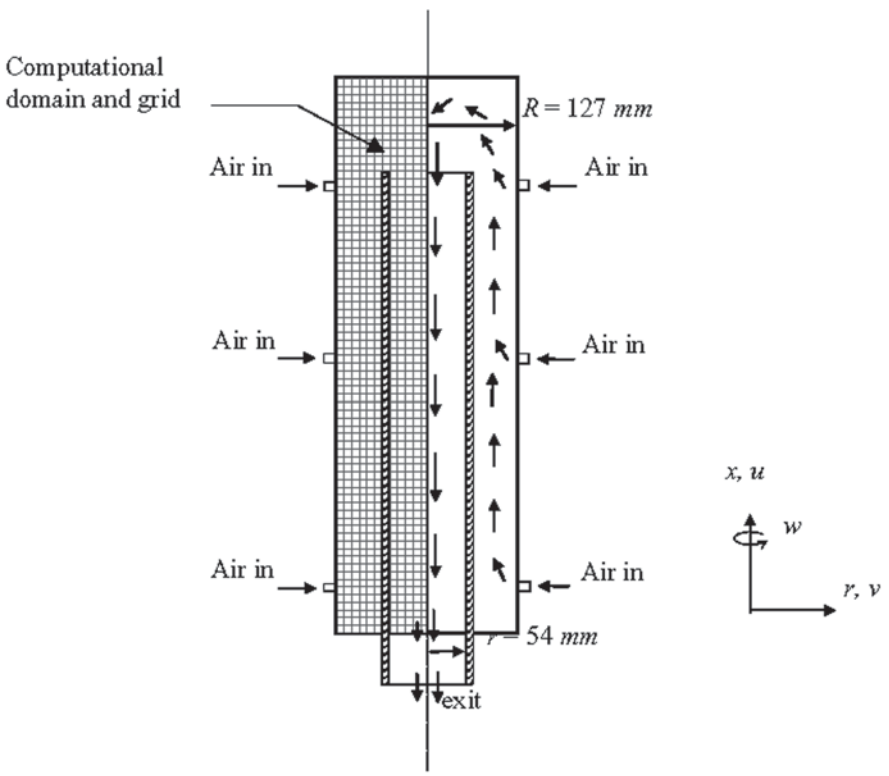

Figure 1 Flow arrangement, computational domain and grid for the vortex combustor (Zhang *et al*., 1992).

(Zhang *et al.*, 1992) in Fig 1. The results of these computations are shown in Figures 2 to 10. The influence of grid mesh distribution and the discretization schemes on the predicted velocity profiles are shown by comparison of the profiles with measurements at ten axial locations, namely, x = 0.051, 0.112, 0.173, 0.234, 0.295, 0.358, 0.42 0.483, 0.544, and 0.605 m in Figures 2 and 3 respectively. The predicted radial profiles of axial and tangential velocities with the k-ε model and the QUICK scheme for different grid densities are presented in Figures 2(a) and 2(b) respectively.

It was seen that all grids other than the coarse one of 30×15 of are very nearly the same results, indicating a grid size of 40×20 or finer to be sufficient to ensure grid-independence of results. The axial and tangential velocity variations in Figures 3(a) and 3(b), respectively, for various numerical schemes along with the measurements showed that, except for minor differences, all three schemes for the convective terms yielded almost the same results. Thus, any of the numerical schemes could be used to calculate flow with adequate accuracy. These figures indicated that the predictions with the k-ε model resulted in poorer agreement with the experimental data. For example, the k-ε model failed to predict the central toroidal recirculation zone and the combined forced and free vortex motion in the upper region of the combustor (at x = 0.544 and 0.605 m).

Predictions of the axial and tangential velocities using the ASM for different grid size distributions were compared with measurements in Figures 4(a) and 4(b) respectively. All three grids (30×15, 40×20 and 47×25 points) yielded similar results, indicating adequate grid-independence. It was interesting to note that a grid-independent solution was achieved with a coarser grid than in the case of the k-ε model. The use of ASM also improved the overall agreement between the predictions and the experimental data. Both the central recirculation zone and the Rankine vortex in the upper cylinder were reasonably well predicted by the ASM.

As for the k-ε model, predictions with the ASM using different numerical schemes did not show significant differences, as could be seen in Figures 5(a) and 5(b) for the axial and tangential velocity profiles respectively. This suggested that for strongly swirling flow (S = 13.9) any of numerical schemes could be used for this vortex flow with adequate accuracy. The effects of the value of β between 0.2 and 0.8 in the ASM on the solutions are presented in Figures 6(a) and 6(b), respectively, for axial and tangential velocity profiles along with measurements. It was found that the optimum value for β was between 0.6 and 0.8. For $\beta < 0.6$, the central recirculation zone

Table 1 Geometry and flow conditions for the vortex chamber (Zhang *et al*., 1992).

Parameter	Magnitude		
Vortex chamber geometry			
chamber inner dia., m		0.25	
chamber height, m		0.66	
centre tube outer dia., m		0.13	
centre tube inner dia., m		0.11	
centre tube height, m		0.51	
Multiple air injection			
nozzle height distribution, m	0.051	0.295	0.483
flow rate distribution, m^3/h	226	226	226
tangential velocity, m/s	24.6	24.6	24.6
air temperature, K	300	300	300

and the Rankine vortex profiles were poorly predicted, probably due to the underestimation of the rotational effect on turbulence. This suggested that using the original ASM (β=0) was not likely to be so effective.

Streamlines and velocity vectors using

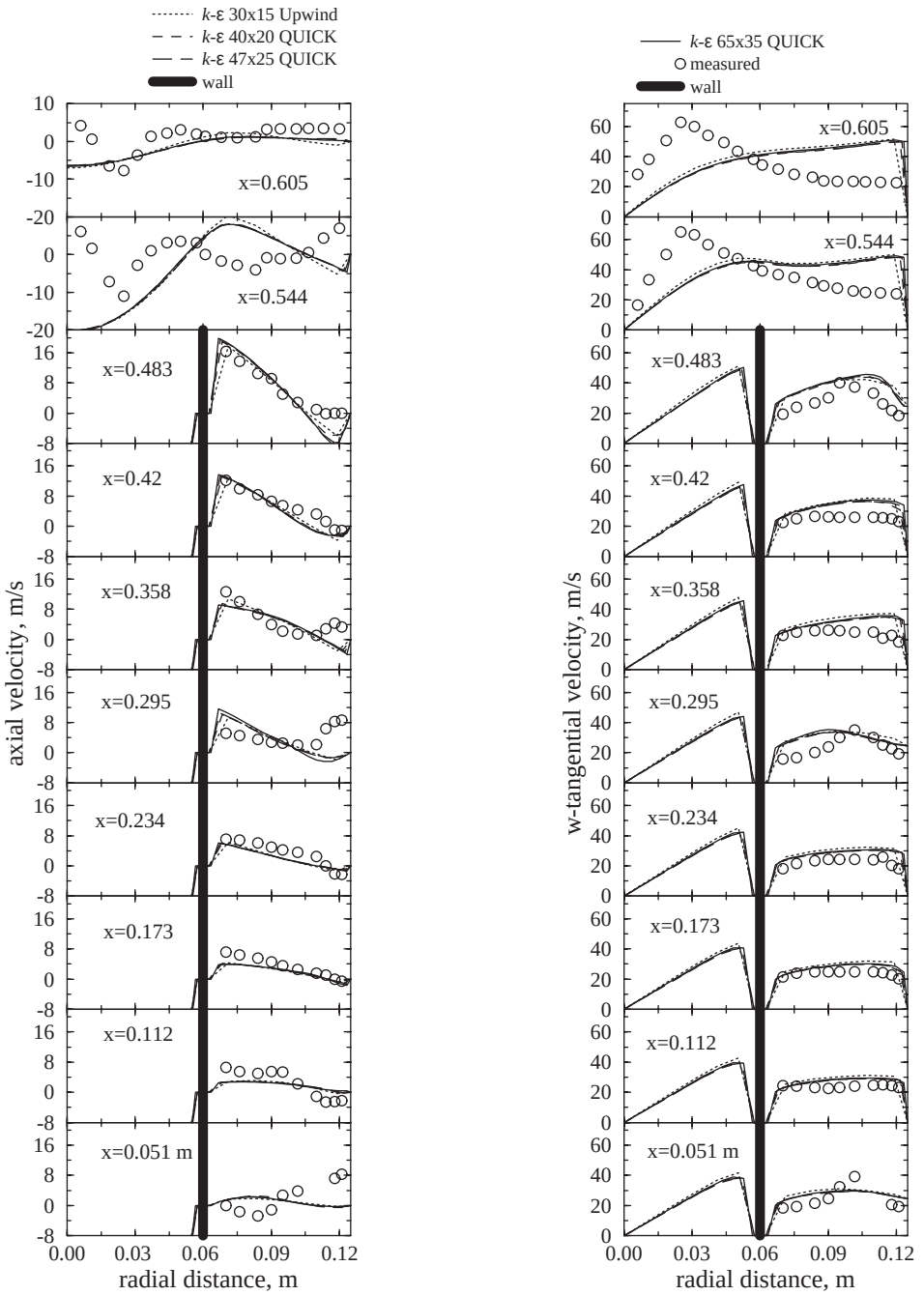

(a) axial velocity (b) tangential velocity

Figure 2 Comparison of the k-ε model predictions using different grid densities with measurements.

the k-ε model are presented in Figures 7 and 8 respectively. There were two recirculation zones: a small one in the lower region of the combustor and the other in the upper region. No experimental data were also provided for comparison. Streamlines and velocity vectors predicted by the ASM are illustrated in Figures 9 and 10 respectively. It was seen that, unlike the k-ε model,

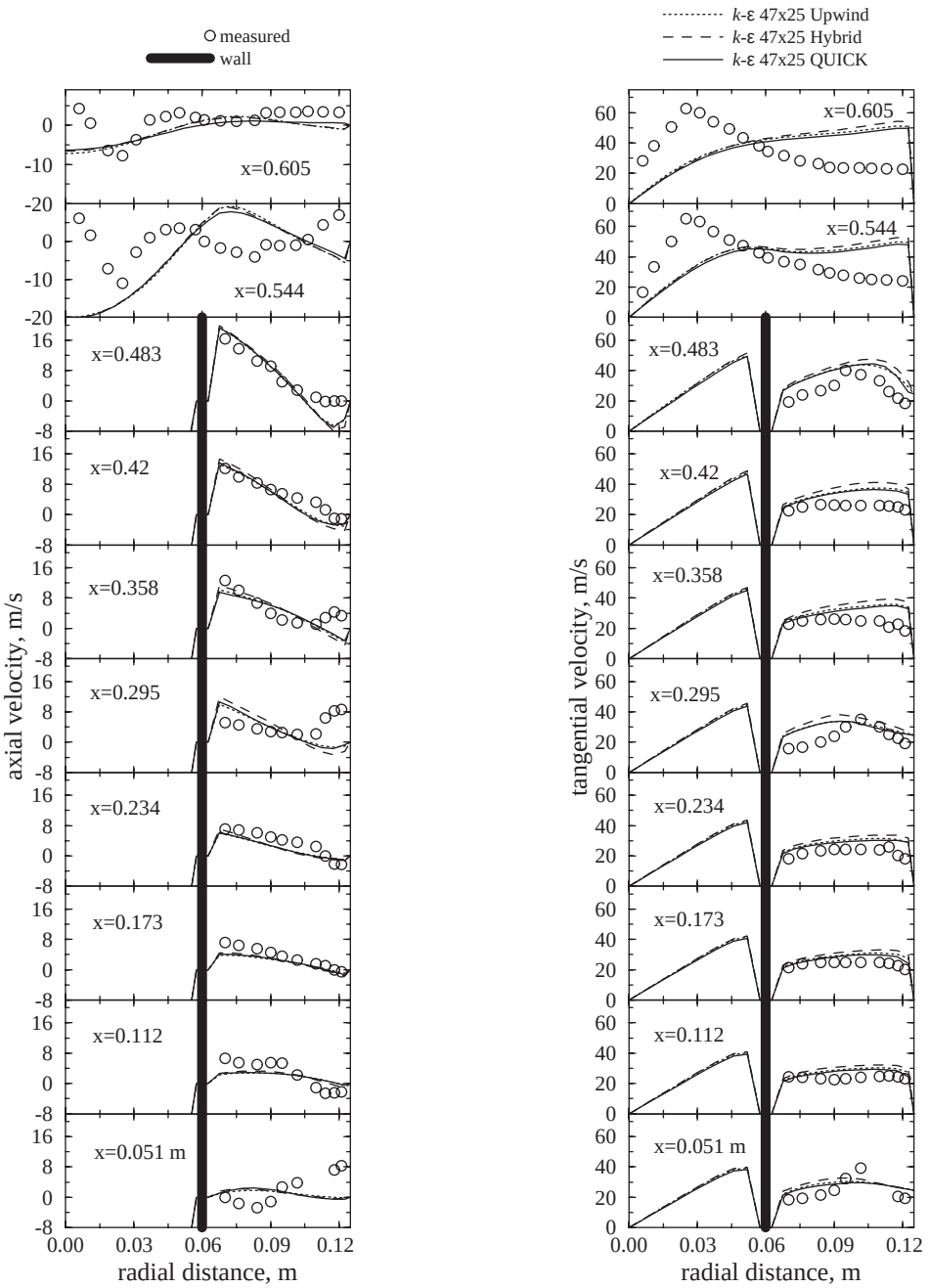

(a) axial velocity (b) tangential velocity

Figure 3 Comparison of the k-ε model predictions using different schemes with measurements.

the ASM, which yields only a single recirculation zone, predicted well the central recirculation zone and the Rankine vortex in the top cylindrical zone of the combustor. Zhang *et al*. (1992) used the same model of the ASM but with a 40×22 grid and a hybrid scheme to calculate this flow. Their

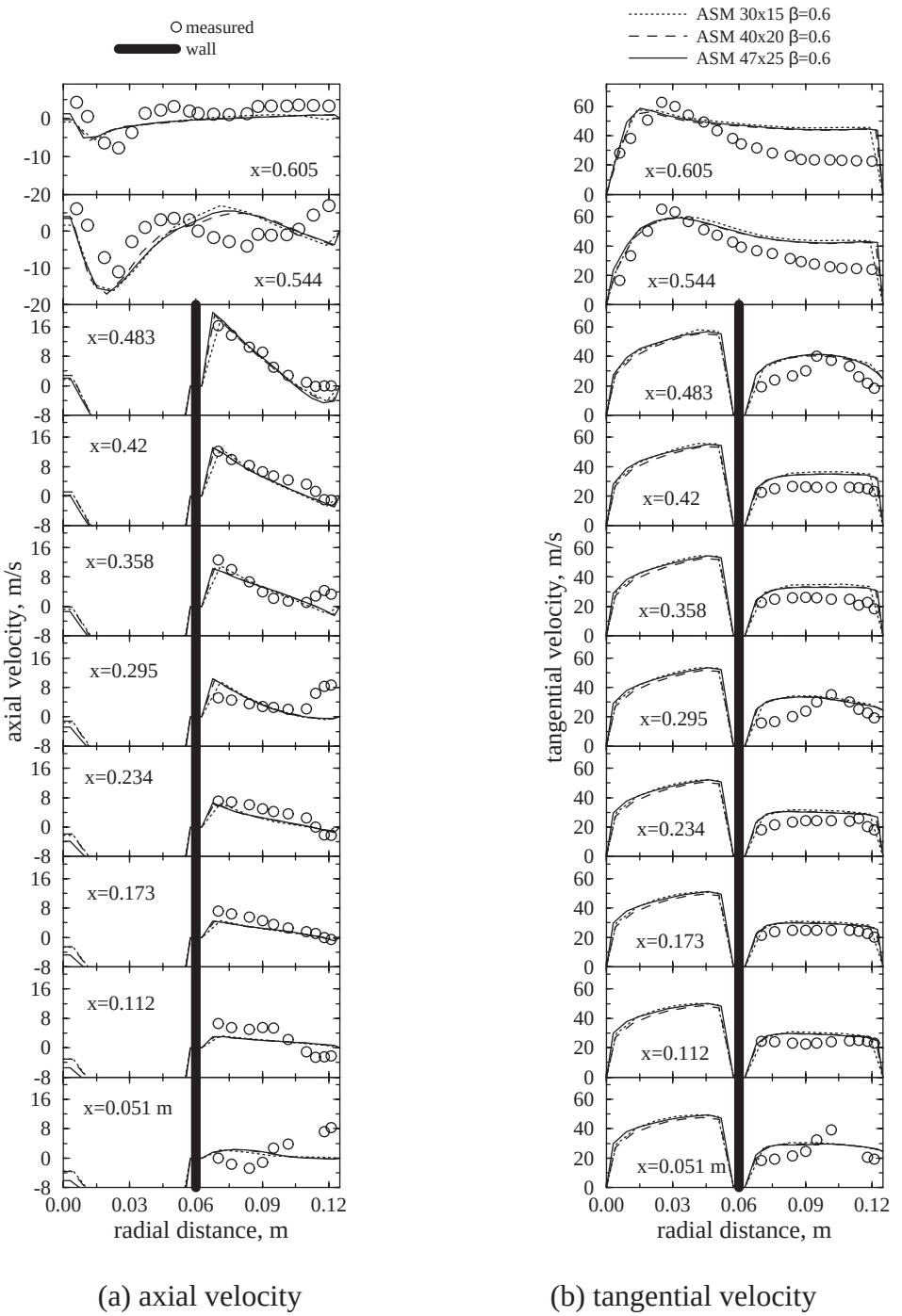

Figure 4 Comparison of the ASM predictions using different grid distributions with measurements.

results with the ASM and the k-ε model were similar to the present calculations, except in the vicinity of the inlet. They found that β = 0.8 was the optimum value. The inlet conditions used by them was not specified and it was likely that they were different from those in this study, and hence leading to slightly different solutions.

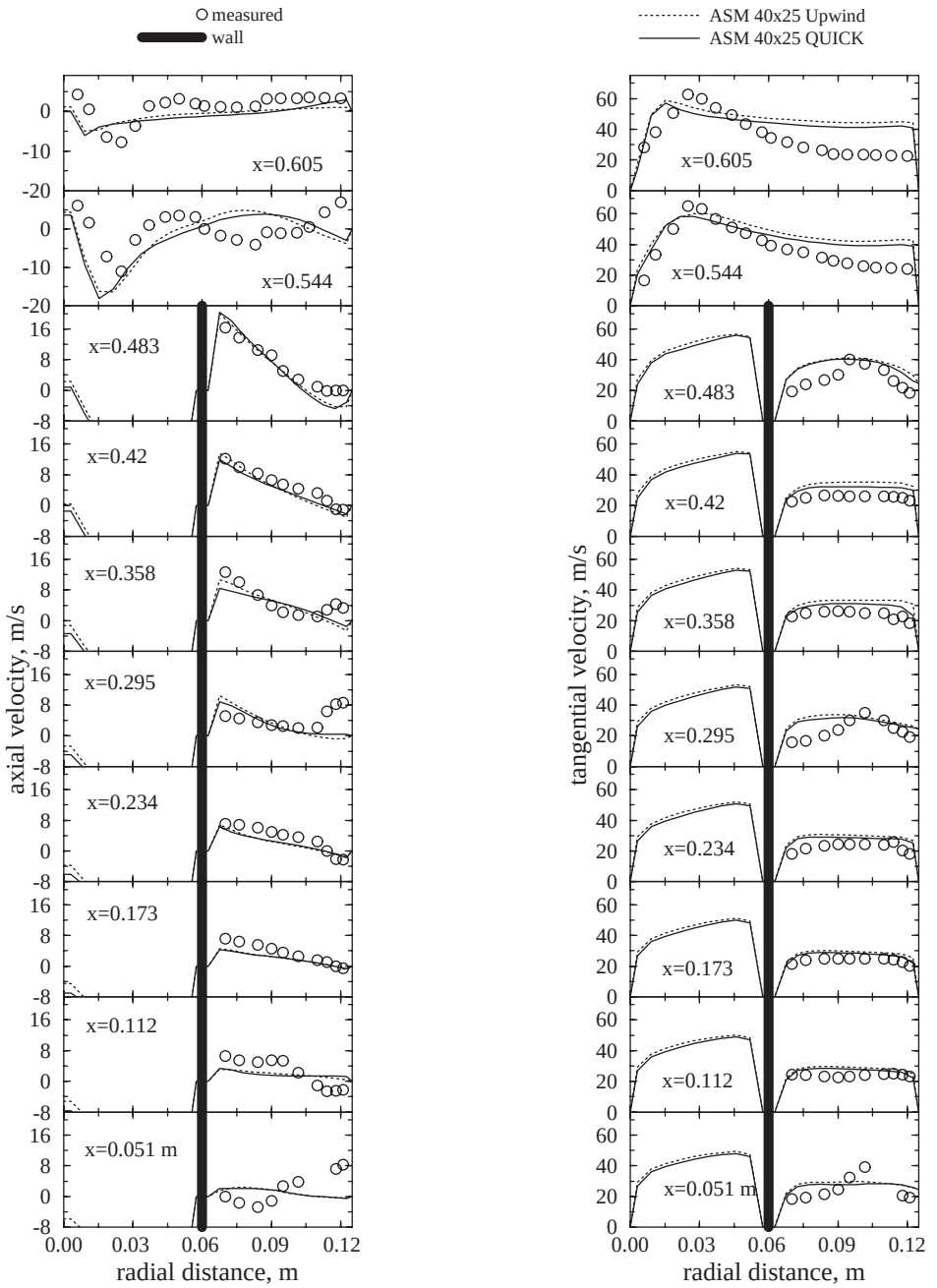

Figure 5 Comparison of the ASM predictions using different schemes with measurements.

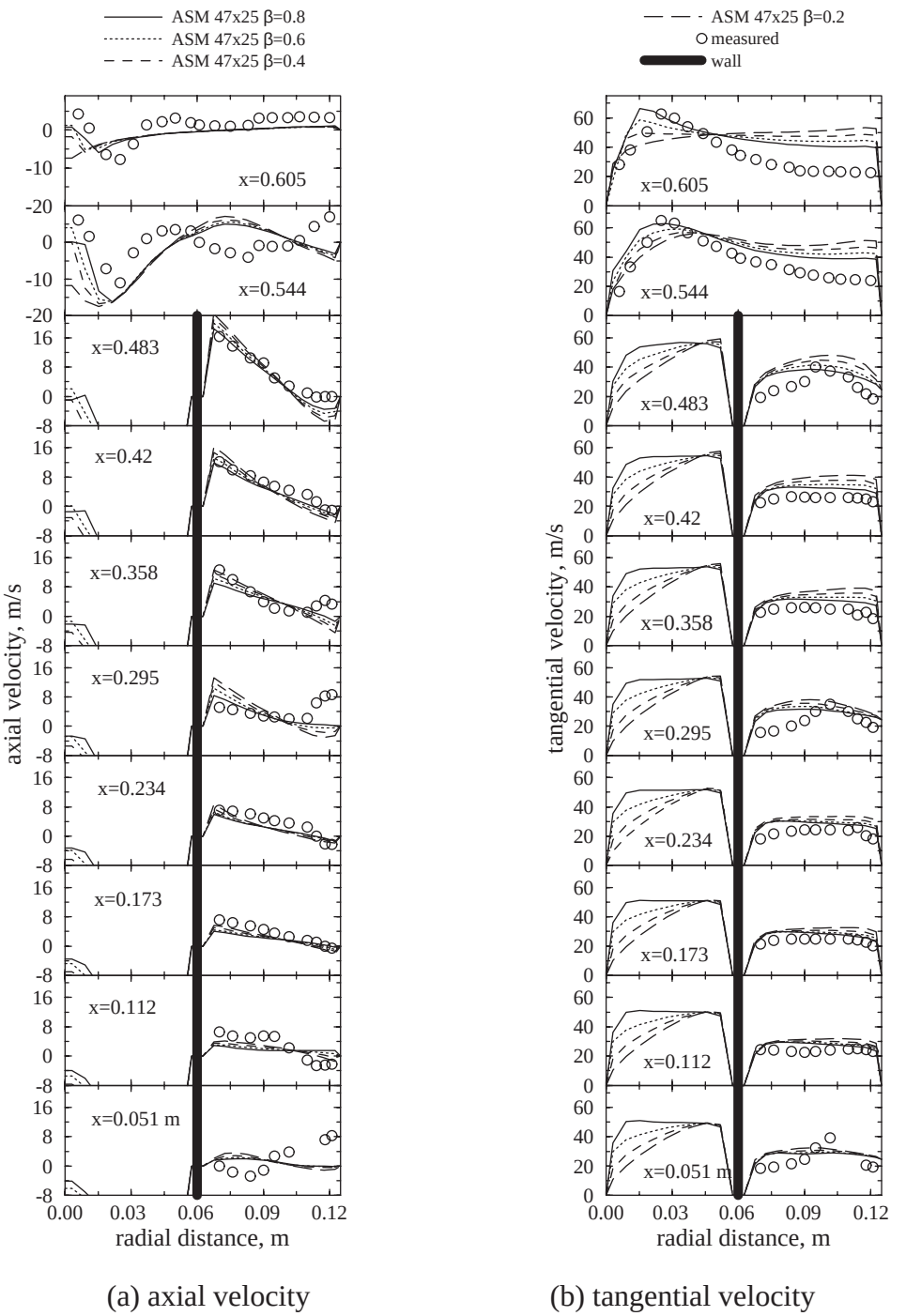

Figure 6 Comparison of the ASM predictions using different β values with measurements.

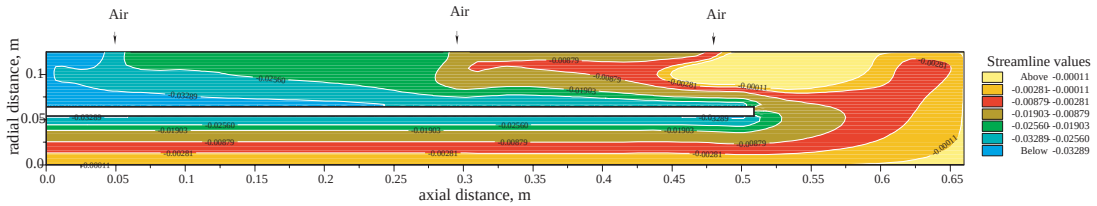

Figure 7 Streamlines predicted by the k-ε model.

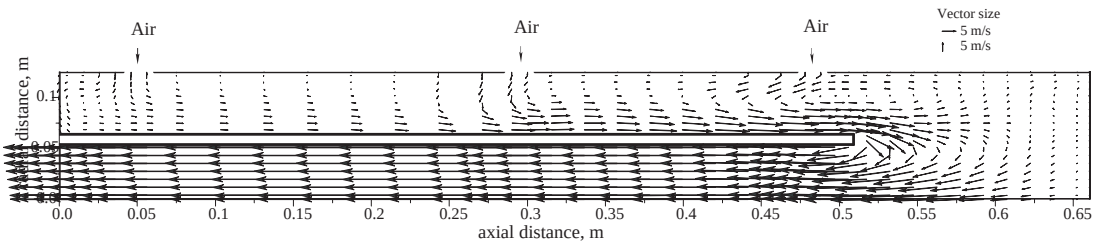

Figure 8 Velocity predicted by the k-ε model.

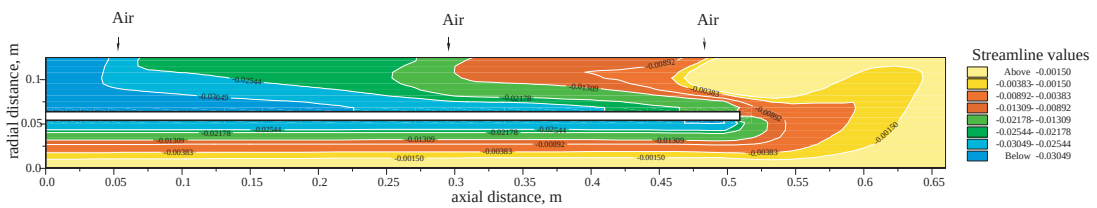

Figure 9 Streamlines predicted by the ASM

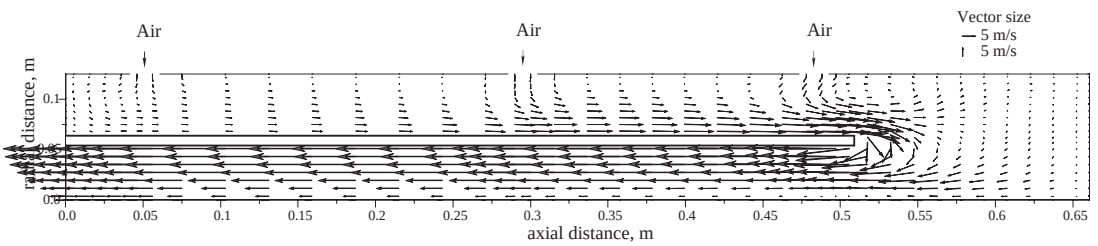

Figure 10 Velocity vectors predicted by the ASM.

CONCLUSIONS

1. The predictions of axial and tangential velocities based on the ASM and k-ε model were in good agreement with available measurements. The computations of the flow showed that the ASM performs slightly better than the standard *k-ε* model in capturing mean flow behaviour.

2. The gas flow in the combustor was characterized as a strongly swirl, re-circulating, and non-isotropic turbulent flow with a dominant tangential velocity component. Local re-circulating flows occured near the injecting nozzles, at the chamber bottom, at the top of the center tube, and in the vortex core.

3. All of the schemes for the convective terms yielded almost the same results which the optimum value of β was found to be in a range from 0.6 to 0.8.

LITERATURE CITED

Boysan F., W.H. Ayers, and J. Swithenbank. 1982. A fundamental mathematical modelling approach to cyclone design. **Trans. Inst. Chem. Eng.** 60: 222-230.

Boysan F., B.C.R. Ewan, J. Swithenbank, and W.H. Ayers. 1983. Experimental and theoretical studies of cyclone separator aerodynamics. *In* **International Chem. Engng. Symp.** 69: 305-319.

Chen C.P. 1986. Calculation of confined swirling jets. **Commu. Appl. Numer. Methods**. 2: 333-338.

Gatski T.B. 1996. Turbulent flows: model equations and solution methodology. *In* **Handbook of Computational Fluid Mechanics**. Academic Press Ltd, London.

Gupta A.K., D.G. Lilley and N. Syred. 1984. **Swirl Flows**. Abacus Press, Turnbridge Wells, England, 10 p.

Hogg, S. and M.A. Leschziner. 1989. Computation of highly swirling confined flow with a Reynolds stress turbulence model. **AIAA J.** 27: 57-63.

Jones, W.P. and A. Pascau 1989. Calculation of confined swirling flows with a second moment closure. **Trans. ASME J. of Fluid Engineering**. 111: 248-255.

Nieh, S. and J. Zhang. 1992. Simulation of the strongly swirling aerodynamic field in a vortex combustor. **Trans. ASME J. of Fluids Engineering** 12: 114.

Patankar, S.V. 1980. **Numerical Heat Transfer and Fluid Flow.** Hemisphere, Washington, D.C., 10 p.

Rodi, W.A. 1976. New algebraic relations for calculating the Reynolds stresses. **Z. Angew. Math. Mech. (ZAMM).** 56: T219-T221.

Zhang, J. and S. Nieh. 1992. Numerical simulation of the effects of center tube and multiple air injection on the gas flow field in a vortex combustor. **Combust. Sci. and Tech.** 88: 43-57.

Zhang, J., S. Nieh, and L. Zhou. 1992. A new version of algebraic stress model for simulating strongly swirling turbulent flows. **J. Numerical Heat Transfer.** Part B, 22: 49-62.